Available online at www.sciencedirect.com
ScienceDirect
Journal of Power Sources 167 (2007) 406–412
JOURNAL OF POWER SOURCES
www.elsevier.com/locate/jpowsour

Performance simulation for an anode-supported SOFC using Star-CD code

Hui-Chung Liu [a,*], Chien-Hsiung Lee [b], Yao-Hua Shiu [b], Ryey-Yi Lee [b], Wei-Mon Yan [a]

[a] *Department of Mechatronic Engineering, Huafan University, Shih-Ting, Taipei 223, Taiwan, ROC*
[b] *Institute of Nuclear Energy Research Atomic Energy Council, Executive Yuan, Taoyuan County 32546, Taiwan, ROC*

Received 20 October 2006; received in revised form 15 February 2007; accepted 15 February 2007
Available online 25 February 2007

Abstract

Experimental activities and computational fluid dynamics (CFD) simulation are presented in this paper for investigating the performance of an anode-supported solid oxide fuel cell (SOFC). The goal of this work is to assess a commercial CFD code, Star-CD with es-sofc module, to simulate the current–voltage (*I–V*) characteristics with respect to the experimental data. Compiled with the geometry of cell test housing, a 3D numerical model and test conditions were established to analyze the anode-supported cell (ASC) performance including current density and temperature distributions, fuel concentration, and fuel utilization. After adjusting parameters in the electrochemical model, the simulation results showed good agreements with the experimental data. The results also revealed that the power density increased while the fuel utilization decreased as the fuel flow rate increased.

Based on the results, this modeling work will be implemented to analyze the distributions of fuel and oxidant gases for the SOFC stack, to minimize the thermal gradients inside the stack, and to optimize the manifold/flow passage in the future.

Keywords: SOFC; Simulation; Modeling; Experiment

1. Introduction

A solid oxide fuel cell (SOFC) is a device that converts chemical energy into electrical power through electrochemical reactions at elevated temperatures. SOFCs offer a potential for high efficiency, fuel flexibility and low air pollution, and the possibility of coupling the integrated gasification combined cycle (IGCC) to develop a SOFC coal-based central power plant with cleanness and higher efficiency.

SOFCs operating at high temperatures have advantages, such as preserving the high oxide-ion conductivity, high kinetic activity without a catalyst, carbon monoxide being a fuel rather than a poison, and the exhausted heat can be recovered to heat incoming fuel and air. On the other hand, high operating temperatures cause some material problems such as stresses at the interfaces due to different thermal expansion coefficients of the SOFC components, and induce performance degradation, resulting in instability and a cost increase.

In the development of the SOFC, planar type designs have received much attention because of the higher power densities compared with tubular-type designs. A planar type anode-supported cell (ASC) with a very thin electrolyte drastically decreases the ionic transport resistance and enables operation at intermediate temperatures to mitigate the extent of the SOFC material problems.

Many experimental and numerical simulation studies were developed to analyze the SOFC cell performance [1–9]. In particular, commercially computational fluid dynamics simulation codes are widely used to analyze complex phenomena. Autissier et al. [10] proved subroutines in the commercial software, FLUENT, to calculate reaction rates, and distributions of current density, gas flow, cell temperature, and fuel concentration in ASC cells. In their research, electrochemical behavior is experimentally fitted on small cells and then applied to complex geometries. The studies of Yakabe et al. [11] adopted a commercial computational fluid dynamics tool, Star-CD, to calculate the detailed SOFC characteristics such as fuel concentrations,

* Corresponding author. Tel.: +886 2 26632102x4011; fax: +886 2 26632102x4013.
E-mail address: d9062004@cat.hfu.edu.tw (H.-C. Liu).

0378-7753/$ – see front matter © 2007 Elsevier B.V. All rights reserved.
doi:10.1016/j.jpowsour.2007.02.033

Nomenclature

A_i	pre-exponential factor
$\bar{c}$	mean constant-volume specific heat
c_p	constant-pressure specific heat
d	thickness
D	mass diffusivity ($m^2\ s^{-1}$)
E	open circuit voltage
E_{act}	activation energy
F	Faraday constant (96,487 C mol^{-1})
F_h	diffusional energy flux
F_m	diffusional flux
h	static enthalpy
H	heat of formation
i	current density ($A\ m^{-2}$)
i_0	exchange current density ($A\ m^{-2}$)
k	electrochemical reaction rate constant
M	molecular weight (g)
P	pressure (Pa)
R	universal gas constant (8.314 J $(mol\ K)^{-1}$)
R_i	resistance
R_m	rate of mass production or consumption
s	source term
T	temperature (K)
V	operating voltage (V)
$\dot{V}$	gas flow rate (ml min^{-1})
Y	mass fraction

Greek letters

ρ	density (kg cm^{-3})
τ	stress tensor

Subscripts

a	anode
c	cathode
eff	effective
H_2	hydrogen
O_2	oxygen
m	mth composition of fuel reactant

Subscripts

0	reference

temperature and current density distributions, etc., through a simplified electrochemical model. Thermal stress calculations were analyzed by another commercial code, ABAQUS. The results showed a co-flow pattern is advantageous to mitigate the temperature differences, and hence to reduce internal stresses. In Yakabe and Sakurai's model [12], the electromotive force counterbalance with the oxygen ions was used to calculate the electric current flow in SOFC. The effects of variations of channel to rib width ratios were investigated. It was found that the current density and contact resistance at the interfaces increased with the channel to rib width ratio, as a result of a smaller contact area between interconnect and electrode. Recknagle et al. [13] used Star-CD to investigate the effects of cell flow configurations,

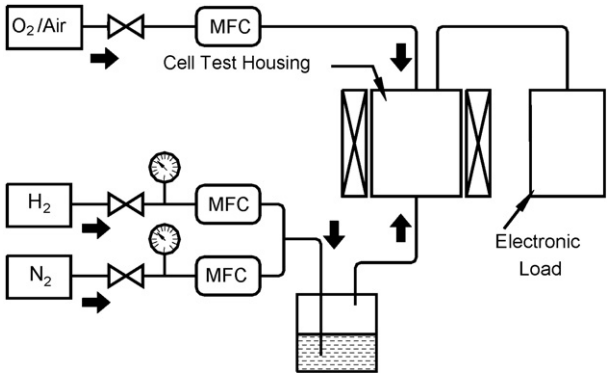

Fig. 1. Schematic diagram of the cell test station.

including co-flow, cross-flow and counter-flow. Under similar conditions in fuel utilizations and average cell temperatures, the co-flow case would yield smaller temperature gradient.

The goal of this work is to verify the accuracy of a commercial CFD code, Star-CD (Version 3.26), with the es-sofc module, in a simulation of the *I–V* characteristics against the experimental data obtained from the cell tests. Based on the geometry of the cell test housing and test conditions, a 3D numerical model of Star-CD was established to analyze the anode-supported cell performance including current density distribution, fuel concentration distribution, and flow utilization.

Section 2 of this paper illustrates the SOFC cell performance experiment established at the Institute of Nuclear Energy Research (INER). Section 3 describes the simulation method for a planar type anode-supported cell including the model geometry, thermo-fluid model and electrochemical model. Section 4 presents simulation results and a comparison with experiment data. Finally, a brief conclusion is given in Section 5.

2. Experimental description

The single-cell test station to investigate the electrochemical characteristics of a planar type SOFC cell has been set up at INER. The schematic diagram of the cell test station is shown in Fig. 1. The test station consists of a gas manifold system, an electronic load module and a single-cell test housing enclosed in a furnace. Hydrogen is humidified and supplied to the anode compartment, and oxygen or air is directed to the cathode side as the oxidant gas. A circular cell of 5 cm diameter was set between fuel and air distributions.

The air and hydrogen from the upper side and lower side separately flowed into the center of the cell electrodes and distributed radically across the cell surfaces. The effective electrode area of test cell was about 20 cm^2. In the test, a heating rate of 1 °C min^{-1} is set. The NiO in the anode was gradually reduced to nickel in situ during the heating-up process with a fuel gas composition of 10% H_2/90% N_2. As the temperature reached to setting point, the H_2 concentration was gradually increased to 100% at steps of 10% for every 30-min period. The cell performance was then carried out at varied fuel concentration and flow rates.

Fig. 2 illustrates two measured characteristics: *I–V* and *I*–power curves for the ASC tests operating at 800 °C with gas

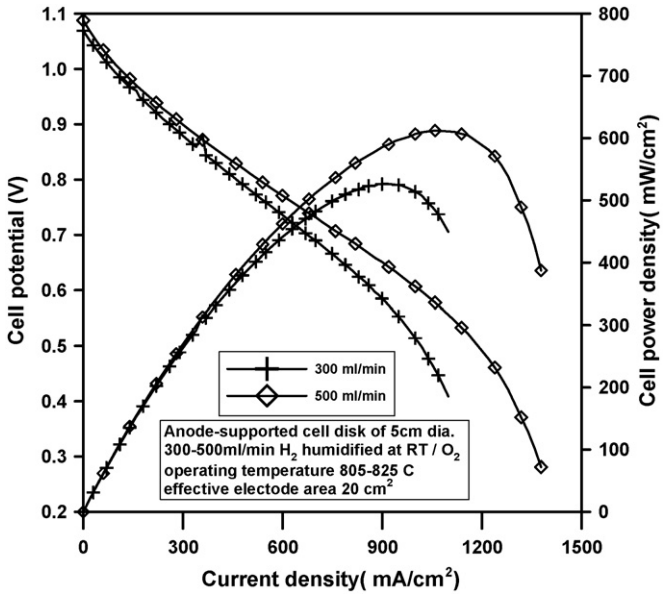

Fig. 2. Effect of fuel gas flow rate on cell performance.

flow rates of 300 and 500 ml min^{-1}, respectively. It reveals that only slight difference of current density for two different gas flow rates in the region of higher cell voltage while the differences expands the decrease of cell voltage. For gas flow rate of 500 ml min^{-1}, the peak power density was 610 mW cm^{-2}, which was about 15% higher than that of 300 ml min^{-1} gas flow rate. These test data of the *I–V* characteristics were used to benchmark the Star-CD simulation.

3. Simulation method

The widely used Star-CD code [11–13] and an advanced electrochemical module es-sofc, developed by the Pacific Northwest National Laboratory (PNNL), were selected to compute the thermal-fluid behavior and the complex electrochemical reaction in a planar type anode-supported cell. The es-sofc module is employed to analyze the distributions of fuel and oxidant to the cell. Additionally, cell voltages and current densities can be subsequently calculated.

3.1. Geometric model

Fig. 3 shows a schematic of the geometric model for a SOFC test cell. The 3D cylindrical model includes the cathode interconnect, platinum mesh, positive-electrolyte-negative (PEN), nickel mesh, and anode interconnect. The gas flow configuration including the ribs produced by horizontal and vertical channels on the anode and cathode interconnects is also shown in Fig. 3. The major geometric data for the input to Star-CD are listed in Table 1.

3.2. Thermo-fluid model

Star-CD code solves the Navier–Stokes equations for each of the computational mesh element in the fluid region. To simplify

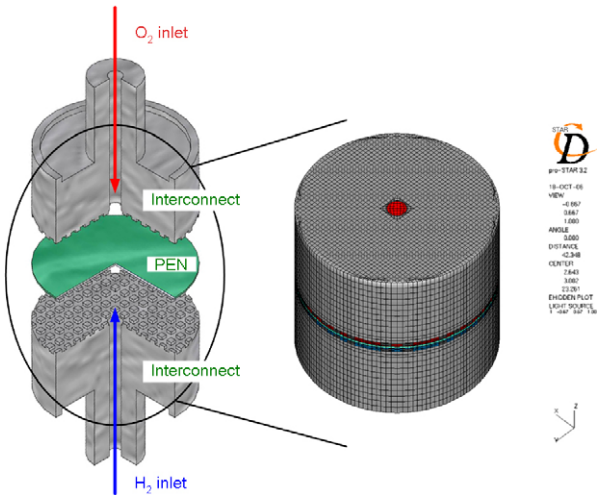

Fig. 3. Simulation modeling of the cylindrical test rig.

cell performance calculations, the following assumptions are made: (1) gas mixtures are modeled as perfect gases; (2) gas flow is steady and laminar everywhere in the cell channels; (3) anode and cathode are considered to be isotropic porous media. Based on those assumptions, the governing equations for the conservation of mass, momentum, enthalpy and species in Star-CD code are illustrated as follows.

Mass equation:

$$\frac{\partial \rho}{\partial t} + \frac{\partial \rho u_j}{\partial x_j} = s_m \tag{1}$$

Momentum equation:

$$\frac{\partial \rho u_i}{\partial t} + \frac{\partial}{\partial x_j}(\rho u_j u_i - \tau_{ij}) = -\frac{\partial P}{\partial x_i} + s_i \tag{2}$$

In the above equations, source terms s_m and s_i represent the sums of the body and other external forces, and τ_{ij} is the stress tensor relative to the velocity gradient. The density of

Table 1
Input parameter for Star-CD

PEN thickness	0.6 mm
Anode thickness	0.575 mm
Electrolyte thickness	0.005 mm
Cathode thickness	0.02 mm
Anode porosity	0.3
Cathode porosity	0.3
Rib thickness	1 mm
Interconnect thickness	24 mm
Operation temperature	1073 K
Operation pressure	1 atm
Relative humidity (both anode and cathode)	100%
Cell temperature	800 °C
Anode fuel	H_2
Cathode fuel	O_2
Fuel inlet temperature (both anode and cathode)	790 °C
Pre-exponential factor, A_i	128
Activation energy, E_{act}	550

fuel mixture is given by the ideal gas law:

$$\rho = \frac{P}{RT}\left(\sum_m \frac{Y_m}{M_m}\right) \tag{3}$$

where Y_m is the mass fraction of a component with molecular weight M_m.
Enthalpy equation:

$$\frac{\partial \rho h}{\partial t} + \frac{\partial}{\partial x_j}(\rho h u_j + F_{h,j}) = \frac{\partial P}{\partial t} + u_j \frac{\partial P}{\partial x_j} + \tau_{ij}\frac{\partial u_i}{\partial x_j} + s_h \tag{4}$$

The specific enthalpy h of the fluid was defined as the sum of the thermal and chemical components:

$$h = c_p T - c_p^0 T^0 + \sum Y_m H_m \tag{5}$$

where H_m is the heat of formation of constituent m; c_p the mean constant-pressure specific heat at temperature T with c_p^0 being the reference specific heat at reference temperature T_0. For solids and constant density fluids, such as liquids, Star-CD solves the transport equation for the specific internal energy e:

$$e = \bar{c}T - \bar{c}^0 T^0 + \sum Y_m H_m \tag{6}$$

where $\bar{c}$ is the constant-volume specific heat.
Species equation:

$$\frac{\partial \rho Y_m}{\partial t} + \frac{\partial}{\partial x_j}(\rho u_j Y_m + F_{m,j}) = R_m \tag{7}$$

where F_m is the diffusional flux component, and R_m is the rate of mass production or consumption during chemical reaction.

3.3. Electrochemical model

In Star-CD, electrochemical reactions and net enthalpy generation are calculated by the advanced electrochemical module, es-sofc. The calculations include combustion of oxygen with hydrogen, the gas–water-shift reaction, the capability for steam reformation of methane and addition of nitrogen leaked into the system. In the computation, a specified current density determines the amount of O_2 from the electrolyte, which is then combusted with H_2 from the electrolyte current ($H_2 + (1/2)O_2 \rightarrow H_2O$).

The two limiting current densities for the chemical reactions can be determined as:

$$i_a = \frac{2FD_{eff}(T)P_{H_2}}{RTd_a} \tag{8}$$

$$i_c = \frac{4FPD_{eff}(T)}{RTd_c}\ln\left(\frac{P_{system}}{P_{system} - P_{O_2}}\right) \tag{9}$$

where $D_{eff}(T)$ is the effective diffusion coefficient, P_{H_2} and P_{O_2} the partial pressures of hydrogen and oxygen, F the Faraday constant, and d_a and d_c are, respectively, the thicknesses of anode and cathode.

Electrical performance is evaluated from the resulting fuel and air compositions. The cell voltage is calculated as:

$$V(i) = V_{Nernst} - V_{Ohmic} - V_{Butler–Volmer} + V_{cathode} + V_{anode} \tag{10}$$

In Eq. (10), V_{Nernst} is the Nernst or open circuit potential, V_{ohmic} the Ohmic potential drop, $V_{Butler–Volmer}$ the Butler–Volmer polarization, $V_{cathode}$ the cathode polarization and V_{anode} is the anode polarization. Each item is determined as:

$$V_{Nernst} = \frac{RT}{4F}\ln\left(\frac{P_{O_2,cathode}}{P_{O_2,anode}}\right) \tag{11}$$

$$V_{Ohmic} = iR_i \tag{12}$$

$$V_{Butler–Volmer} = \frac{RT}{\alpha F}\sinh^{-1}\left(\frac{i}{2i_0}\right) \tag{13}$$

$$V_{cathode} = \frac{RT}{4F}\ln\left(1 - \frac{i}{i_c}\right) \tag{14}$$

$$V_{anode} = \frac{RT}{2F}\ln\left(1 - \frac{i}{i_a}\right) \tag{15}$$

In Eq. (13), the exchange current density i_0 corresponds to the dynamic electron transfer rate at equilibrium and can be expressed as [14]:

$$i_0 = A_i \cdot \exp\frac{-E_{act}}{RT} \tag{16}$$

In Eq. (16), the pre-factor, A_i and the activation energy E_{act} are properties specific to the electrode–electrolyte interface in the electrochemical model. In present study, the two parameters were calibrated to fit one of the experimental I–V curves.

The entire meshed volume of the model is divided into about 95,000 cells by preprocessing software Gridgen. The solution to the governing equations is performed using Star-CD by dividing the model domain into a number of cells as control volumes. In the finite volume method, the governing equations are numerically integrated over each of these computational cells or control volumes. The finite volume method exploits a collocated cell-centered variable arrangement, where all dependent variables and material properties are stored at the cell center. The average value of any quantity within a control volume is given by its value at the cell center. The model yields for a set of boundary conditions in about 2000 iterations.

4. Results and discussion

The performance curves are shown in Fig. 4. In this work, the experimental results of 500 ml min^{-1} gas rate were used to speculate the values of A_i and E_{act} in the numerical model. In Fig. 4(a), a maximum of 9% average current density difference is found between simulation results and experimental data obtained from cell tests, which indicates a good agreement between simulation and experiment results at cell voltage from 1 to 0.6 V. Based on this model, another 300 ml min^{-1} gas flow rate is simulated with the same parameters of A_i and E_{act} (see

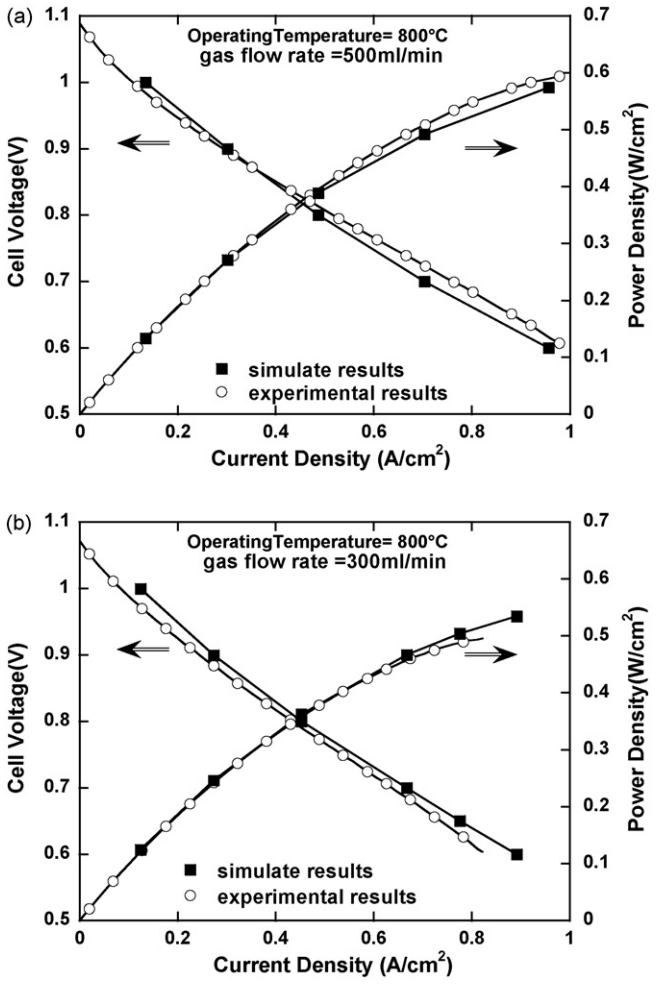

Fig. 4. Comparison between experimental and simulate results. (a) $\dot{V} = 500\,\mathrm{ml\,min^{-1}}$ and (b) $\dot{V} = 300\,\mathrm{ml\,min^{-1}}$.

Table 1) to verify the reliability of those parameters on different gas flow rate. Fig. 4(b) displays the maximum current density difference is about 10% in the comparison of cell performance curves between experimental and simulation results at 300 ml min^{-1} gas flow rate. From Fig. 4, the adjusting parameters in Star-CD electrochemical model simulations are found to have a good agreement in comparison with the experimental data. The results also show that the cell performance is improved with increased gas flow rate.

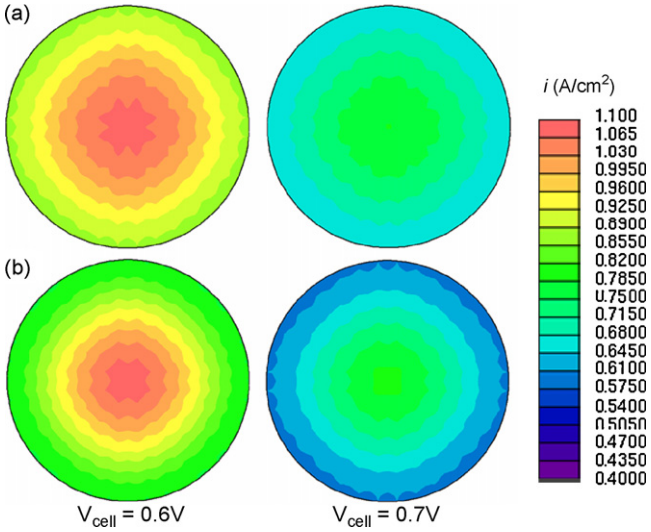

Fig. 6. Current density distribution in PEN at different cell voltages. (a) $\dot{V} = 500\,\mathrm{ml\,min^{-1}}$ and (b) $\dot{V} = 300\,\mathrm{ml\,min^{-1}}$.

In order to investigate the fluid characteristics of fuel, the velocity distribution in anode-side at operating voltage 0.7 V with $\dot{V} = 500\,\mathrm{ml\,min^{-1}}$ and $\dot{V} = 300\,\mathrm{ml\,min^{-1}}$ are, respectively, presented in Fig. 5(a and b). Fuel flows into the cell from the inlet at the center of interconnect. After gas impinging on PEN, the velocity vector demonstrates a radial distribution because of an open-outlet flow field and group of pin-fins design. As shown in Fig. 5, a higher local velocity is found in $\dot{V} = 500\,\mathrm{ml\,min^{-1}}$. For the open-outlet flow field design, uniform velocity vector can be found in the outlet of the flow field for similar long flow routes.

The operating voltage effects on the local current density distributions at $\dot{V} = 500\,\mathrm{ml\,min^{-1}}$ and $\dot{V} = 300\,\mathrm{ml\,min^{-1}}$ are shown in Fig. 6. Results in Fig. 6 show that current density distributions decrease annularly from center to outlet as a result

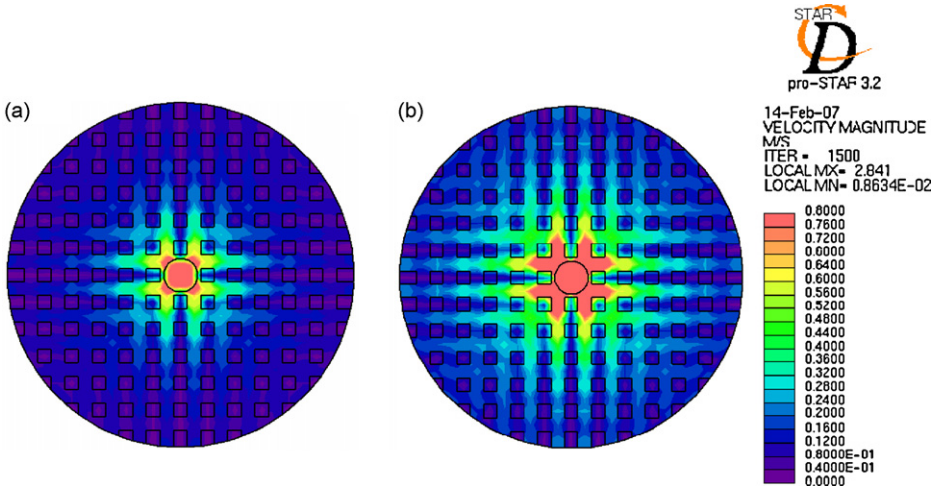

Fig. 5. Velocity vector distribution in anode-side at $V_{cell} = 0.7$ V. (a) $\dot{V} = 500\,\mathrm{ml\,min^{-1}}$ and (b) $\dot{V} = 300\,\mathrm{ml\,min^{-1}}$.

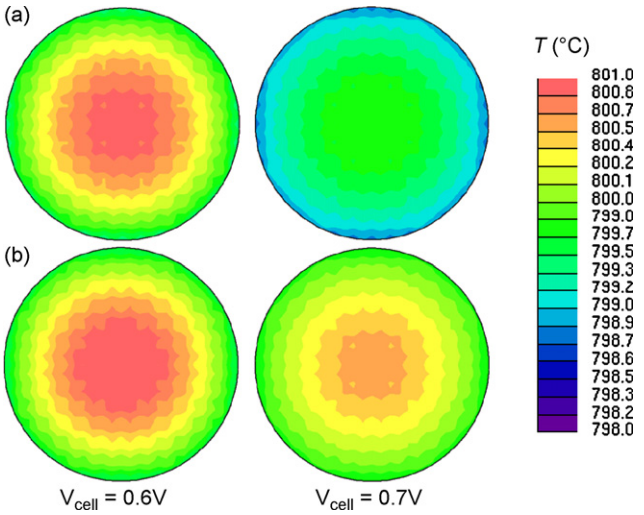

Fig. 7. Temperature distribution in PEN at different cell voltages. (a) $\dot{V} = 500\,\mathrm{ml\,min^{-1}}$ and (b) $\dot{V} = 300\,\mathrm{ml\,min^{-1}}$.

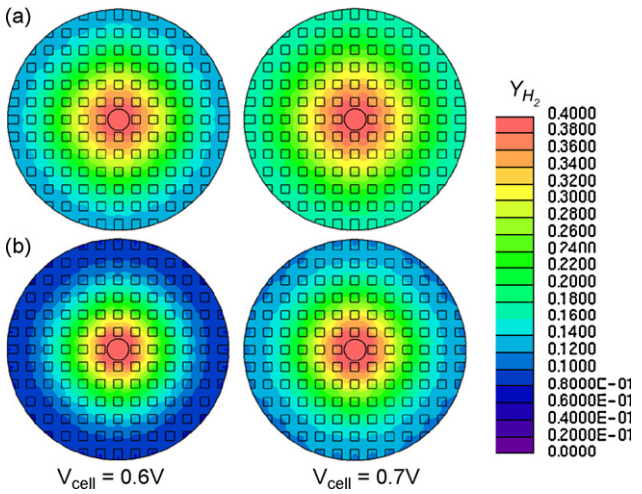

Fig. 8. Mass fraction distribution of hydrogen at anode-side porous media at different cell voltages. (a) $\dot{V} = 500\,\mathrm{ml\,min^{-1}}$ and (b) $\dot{V} = 300\,\mathrm{ml\,min^{-1}}$.

of decrease of fuel concentration by electrochemical reaction. According to the velocity vector distribution, a slight improvement of current density is found in the channel area than in the rib area, since fuel diffuses into electrodes directly in channel areas, but fuel has a longer diffusion-path to get into electrode to react in rib areas. By comparing the ordinates in Fig. 6(a and b), it indicates that the variations in the local current density are more noticeable in the cases of lower operating voltage. The electrochemical reaction is expected to be stronger at a lower operating voltage and thus a higher operating current density.

Heat generation from electrochemical reaction of SOFC is a significant issue in the development of SOFC. Fig. 7 shows temperature distributions in PEN area at different cell voltages. The predictions in Fig. 7 disclose that the temperature gradient increases gradually with cell voltage decrease because of higher electrochemical reaction. In this study, the maximum difference in temperature distribution is less than 3 °C. Inspection of Fig. 7 indicates that weak temperature peaks distribute on the area below channel area as a result of higher electrochemical reaction rate with higher fuel gas distributions. It is interesting to note that the temperature distributions on gas flow rate are contrary to the distribution of current density and fuel gas mass fraction because a low temperature fuel and high fuel gas velocity (formed by a higher gas flow rate) in the flow-field can carry more heat out. In addition, from the results we can find that PEN temperature depends on the inlet temperature of cathode gas due to a larger specific heat.

In the study of fuel transport in SOFC, exploring the distributions of the fuel gases is important to the design of SOFC flow field. To this end, the cell voltage effects on the local distributions of oxygen and hydrogen mass fractions at the interface between interconnect and electrode are presented in Figs. 8 and 9, respectively. This can be made plausible by noting that, for a lower operating voltage, the electrochemical reaction is faster and thus consumes more fuel gases both in anode and cathode. Careful inspection of Fig. 8(a) indicates that a slightly higher hydrogen mass fraction can be found in channel area. The higher hydrogen mass fraction could provide more chance to let hydrogen react in electrode to lead a better cell performance. In a lower gas flow rate condition, the obvious reduction on hydrogen mass fraction is displayed in Fig. 8(b). The result reflects the lower cell current density distribution as shown in Fig. 6. Similar results could be found on oxygen mass fraction in Fig. 9, but the advance on the mass fraction in channel here is more noticeable than that in hydrogen.

Fuel utilization rate is an important parameter for the development of SOFC. To examine the gas flow rate effect on fuel consumption, Fig. 10 shows the comparison of fuel utilization rate between $\dot{V} = 500\,\mathrm{ml\,min^{-1}}$ and $\dot{V} = 300\,\mathrm{ml\,min^{-1}}$ where the fuel utilization rate is defined as:

$$\text{Fuel utilization rate} = \left(1 - \frac{\text{fuel}_{\text{out}}}{\text{fuel}_{\text{in}}}\right) \times 100\% \qquad (17)$$

From Fig. 10 we can find that the fuel utilization rate increases with the decrease in cell voltage for a higher electrochemical reaction rate. It is interesting to note that the fuel utilization rate

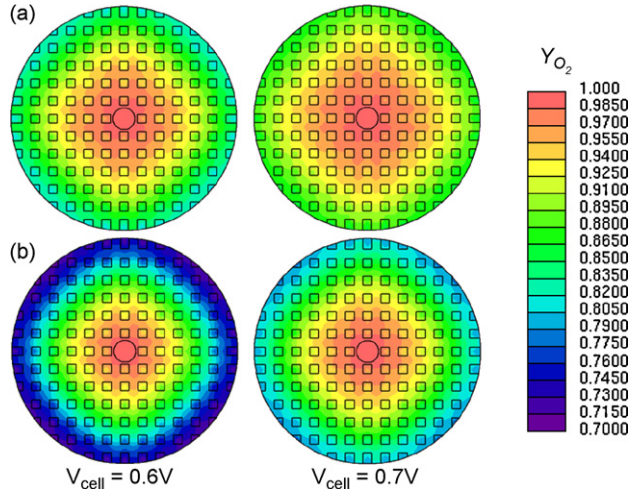

Fig. 9. Mass fraction distribution of oxygen at cathode-side porous media with difference cell voltage. (a) $\dot{V} = 500\,\mathrm{ml\,min^{-1}}$ and (b) $\dot{V} = 300\,\mathrm{ml\,min^{-1}}$.

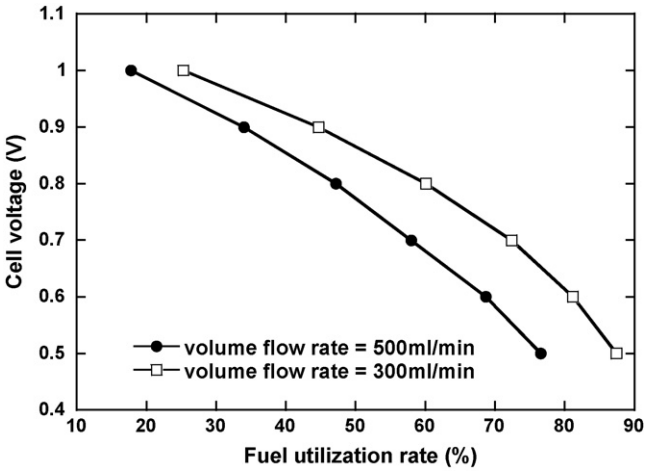

Fig. 10. Comparison of fuel utilization rate between $\dot{V} = 500\,\mathrm{ml\,min^{-1}}$ and $\dot{V} = 300\,\mathrm{ml\,min^{-1}}$.

decreases while gas flow rate increases. With the same electrochemical reaction area, higher fuel gas flow rate could provide more fuel to react, but also more chemical products are generated, which induces resistance for fuel diffusing into electrodes to join the chemical reaction. The mechanism also explains the cell performance curves in Fig. 2. The slight current density difference at high cell voltage with different fuel gas flow rate is found since higher fuel utilization in lower fuel gas flow rate.

5. Conclusions

The fluid dynamics simulation code, Star-CD with es-sofc, was used to verify the performance curve of a solid oxide fuel cell acquired by experimental measurement. Good agreements have been demonstrated between the simulations and the experimental data. The detailed characteristics (include current density and fuel concentration distribution, and fuel utilization) of SOFC were investigated in this study. What follows are the major findings:

1. The cell performance was improved with volume flow rate increase; a lower volume flow rate means a lower fuel inlet velocity and a lower electrochemical reaction rate.
2. Higher fuel mass fractions allow the hydrogen to react in the electrode better for improved cell performance.
3. Fuel utilization becomes worse as the fuel flow rate increases, while the power density is higher.

This modeling work has the potential to be further extended to analyze the distributions of fuel and oxidant for the SOFC stack to investigate the mitigation thermal gradients along with temperature prediction for the calculation of thermally induced stresses, and manifold/flow passage optimization in the future.

Acknowledgement

This study was supported by the Institute of Nuclear Energy Research Atomic Energy Council, Executive Yuan, Taoyuan County 32546, Taiwan, ROC.

References

[1] M. Dokiya, Solid State Ionics (2002) 383–392.
[2] T.-L. Wen, D. Wang, H.Y. Tu, M. Chen, Z. Lu, Z. Zhang, H. Nie, W. Hua, J. Power Sources (2002) 399–404.
[3] X. Jacques-Bedard, T.W. Napporn, R. Roberge, M. Meunier, J. Power Sources 153 (2006) 108–113.
[4] Y. Inui, A. Urata, N. Ito, T. Nakajima, T. Tanaka, Energy Conver. Manage. 47 (2006) 1738–1747.
[5] Y. Inui, N. Ito, T. Nakajima, A. Urata, Energy Conver. Manage. 47 (2006) 2319–2328.
[6] M. Yokoo, T. Take, J. Power Sources 137 (2004) 206–215.
[7] T. Araki, T. Ohba, S. Takezawa, K. Onda, Y. Sakaki, J. Power Sources 158 (2006) 52–59.
[8] A. Selimovic, M. Kemm, T. Torisson, M. Assadi, J. Power Sources 145 (2005) 463–469.
[9] J.J. Hwang, C.K. Chen, D.Y. Lin, J. Power Sources 143 (2005) 75–83.
[10] N. Autissier, D. Larrain, J. Van herle, D. Favrat, J. Power Sources 131 (2004) 313–319.
[11] H. Yakabe, T. Ogiwara, M. Hishinuma, I. Yasuda, J. Power Sources 102 (2001) 144–154.
[12] H. Yakabe, T. Sakurai, J. Power Sources 174 (2004) 295–602.
[13] K.P. Recknagle, R.E. Williford, L.A. Chick, D.R. Rector, M.A. Khaleel, J. Power Sources 113 (2003) 109–114.
[14] M.A. Khaleel, Z. Lin, P. Singh, W. Surdoval, D. Collin, J. Power Sources 130 (2004) 136–148.